Icy moons in the Solar System

Klára Kalousová
klara.kalousova@mff.cuni.cz

Department of Geophysics, Faculty of Mathematics and Physics
Charles University, Prague

Selected chapters on astrophysics (NAST021)
October 15, 2019
room TAU, 14:50–16:20

Course overview

1. Motivation - why do we study icy moons.
   History of exploration - telescope observations, spacecraft missions.
   Surface characteristics - composition, age, and morphology.

2. Interior structure - layered models: from gravity, shape, composition.
   Hydrosphere structure - H_2O phase diagram, presence of oceans.
   Preferred models for selected satellites.

3. Dynamics of the different planetary layers.
   Thermal evolution - heat sources, heat transfer.
   Melting/crystallization, anti-freezers.
   Implications for the long-term stability of subsurface oceans.

4. Selected applications.
   Overview of future missions.

Course overview

1. Motivation - why do we study icy moons.
   History of exploration - telescope observations, spacecraft missions.
   Surface characteristics - composition, age, and morphology.

2. Interior structure - layered models: from gravity, shape, composition.
   Hydrosphere structure - H_2O phase diagram, presence of oceans.
   Preferred models for selected satellites.

3. Dynamics of the different planetary layers.
   Thermal evolution - heat sources, heat transfer.
   Melting/crystallization, anti-freezers.
   Implications for the long-term stability of subsurface oceans.

4. Selected applications.
   Overview of future missions.

Habitability requirements

1. material: C, H, N, O, P, S (~98% of bio molecules on Earth)
2. solvent to speed up reactions - liquid water, ...?
3. energy source to sustain metabolism
4. stable environment

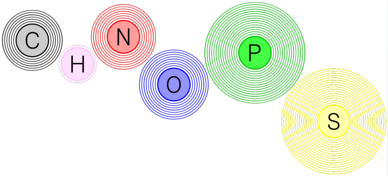



Habitability requirements

1. material: C, H, N, O, P, S (~98% of bio molecules on Earth)
2. solvent to speed up reactions - liquid water, ...?
3. energy source to sustain metabolism
4. stable environment

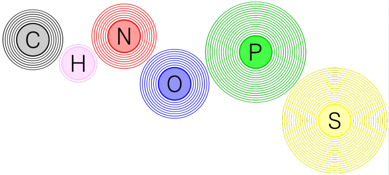

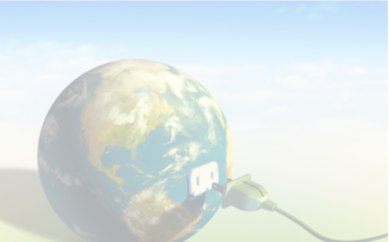

Habitability requirements

1. material: C, H, N, O, P, S (~98% of bio molecules on Earth)
2. solvent to speed up reactions - liquid water, ...?
3. energy source to sustain metabolism
4. stable environment

→ goal of interior structure modeling is to characterize the ocean and the water/rock interface

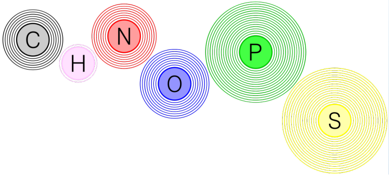

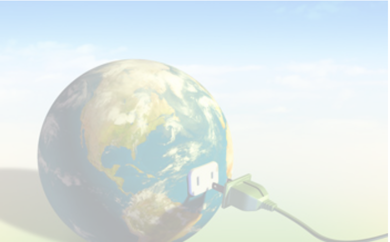

Interior structure of the Earth

- layered - spherical shells (crust, mantle, outer & inner core)
- layering inferred using the travel times of seismic waves:
- body waves: longitudinal P-waves, shear S-waves
- velocity different in each layer, no shear waves through outer core
- reflections & refractions

+ other waves (surface waves, free oscillations, ...)

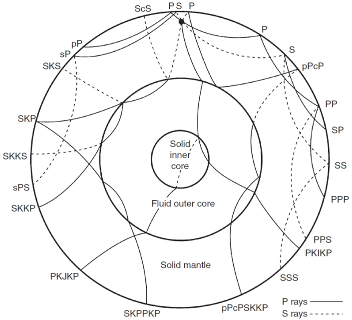

Stein & Wysession (2003)

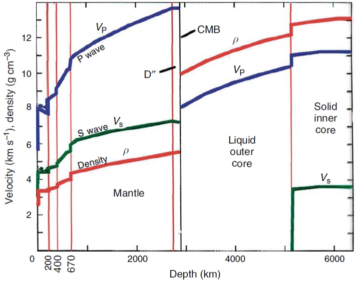

Preliminary Reference Earth Model (*Dziewonski & Anderson*, 1981)

Interior structure of icy moons
(*Hussmann* +, 2015)

- no measurements by seismic network → main clues:

1. radius (size) and mass
2. gravity field
3. rotational state and shape
4. magnetic field
5. surface temperatures and heat flow
6. composition of surface and atmosphere
7. activity at the surface

Interior structure of icy moons

(*Hussmann* +, 2015)

- no measurements by seismic network → main clues:

1 radius (size) and mass

2 gravity field

3 rotational state and shape

4 magnetic field

5 surface temperatures and heat flow

6 composition of surface and atmosphere

7 activity at the surface

- mass + size → average density (important indicator of composition)

Interior structure of icy moons

(*Hussmann* +, 2015)

- no measurements by seismic network → main clues:

1 radius (size) and mass
2 gravity field
3 rotational state and shape
4 magnetic field
5 surface temperatures and heat flow
6 composition of surface and atmosphere
7 activity at the surface

- mass + size → average density (important indicator of composition)
- size + mass + gravity field → moment of inertia (MoI)

Interior structure of icy moons

(*Hussmann* +, 2015)

- no measurements by seismic network → main clues:

1 radius (size) and mass

2 gravity field

3 rotational state and shape

4 magnetic field

5 surface temperatures and heat flow

6 composition of surface and atmosphere

7 activity at the surface

- mass + size → average density (important indicator of composition)
- size + mass + gravity field → moment of inertia (MoI)
- density + MoI → simple structural models of interior

Interior structure of icy moons

(*Hussmann* +, 2015)

- no measurements by seismic network → main clues:

1 radius (size) and mass

2 gravity field

3 rotational state and shape

4 magnetic field

5 surface temperatures and heat flow

6 composition of surface and atmosphere

7 activity at the surface

- mass + size → average density (important indicator of composition)
- size + mass + gravity field → moment of inertia (MoI)
- density + MoI → simple structural models of interior
- shape - can further confirm/reject the model (consistent or not)

Size, shape, mass, and gravitational field - measurements

(*Hussmann* +, 2015; *Schubert* +, 2009)

size

- direct observations of satellite's surfaces by spacecraft imaging systems and ground-based telescopes → physical size
- radius of Titan's solid surface buried beneath 100s km of atmosphere first revealed by radio occultation performed by Voyager 1

Size, shape, mass, and gravitational field - measurements

(*Hussmann* +, 2015; *Schubert* +, 2009)

size

- direct observations of satellite's surfaces by spacecraft imaging systems and ground-based telescopes → physical size
- radius of Titan's solid surface buried beneath 100s km of atmosphere first revealed by radio occultation performed by Voyager 1

shape

- from pictures of the moon acquired by the spacecraft imaging system
- radar altimeter (Titan)

Size, shape, mass, and gravitational field - measurements

(*Hussmann* +, 2015; *Schubert* +, 2009)

size

- direct observations of satellite's surfaces by spacecraft imaging systems and ground-based telescopes → physical size
- radius of Titan's solid surface buried beneath 100s km of atmosphere first revealed by radio occultation performed by Voyager 1

shape

- from pictures of the moon acquired by the spacecraft imaging system
- radar altimeter (Titan)

mass

1. visual observations of satellite motions (Earth-based / spacecraft)

→ identification of mutual gravitational interactions among satellites or between satellites and the parent planet

Size, shape, mass, and gravitational field - measurements

(*Hussmann* +, 2015; *Schubert* +, 2009)

size

- direct observations of satellite's surfaces by spacecraft imaging systems and ground-based telescopes → physical size
- radius of Titan's solid surface buried beneath 100s km of atmosphere first revealed by radio occultation performed by Voyager 1

shape

- from pictures of the moon acquired by the spacecraft imaging system
- radar altimeter (Titan)

mass & gravitational field (2)

1 visual observations of satellite motions (Earth-based / spacecraft)

→ identification of mutual gravitational interactions among satellites or between satellites and the parent planet

2 radio tracking of the spacecraft path during the moon flyby

→ gravitational pull on spacecraft → acceleration/decceleration

→ Doppler shift of radio communication signal recorded by Earth's DSN

→ Doppler data inversion → characteristics of gravitational field

Average density

(*Hussmann* +, 2015)

- mass + size → average density $\rho = \frac{3M}{4\pi R^3}$

→ important indicator of composition

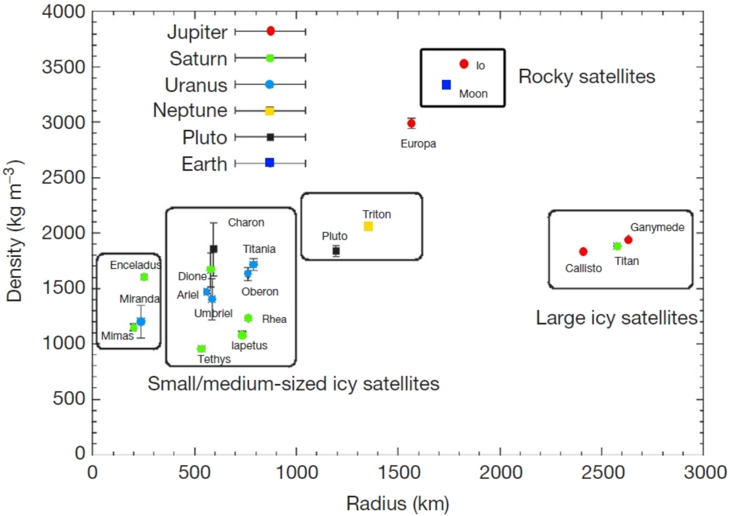

Average density and ice mass fraction

(*Hussmann* +, 2015)

- main composition (~abundances of outer solar system nebula)
  - rock (including iron): olivine $(Mg^{2+}, Fe^{2+})_2SiO_4$, pyroxenes $XY(Si,Al)_2O_6$, serpentines $(Mg,Fe)_3Si_2O_5(OH)_4$, ...
  - nonporous ice/water

Average density and ice mass fraction

(*Hussmann* +, 2015)

- main composition (~abundances of outer solar system nebula)
  - rock (including iron): olivine $(Mg^{2+},Fe^{2+})_2SiO_4$, pyroxenes $XY(Si,Al)_2O_6$, serpentines $(Mg,Fe)_3Si_2O_5(OH)_4$, ...
  - nonporous ice/water
- density in each layer ~ constant (neglect of compression effects)

$$M = \frac{4}{3}\pi\rho R^3 = M_r + M_i = \rho_r V_r + \rho_i V_i = \frac{4}{3}\pi\left[\rho_r R_r^3 + \rho_i\left(R^3 - R_r^3\right)\right]$$

$$\rho R^3 = \rho_r R_r^3 + \rho_i\left(R^3 - R_r^3\right)$$

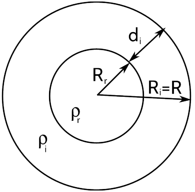

Average density and ice mass fraction

(*Hussmann* +, 2015)

- main composition (~abundances of outer solar system nebula)
  - rock (including iron): olivine $(Mg^{2+},Fe^{2+})_2SiO_4$, pyroxenes $XY(Si,Al)_2O_6$, serpentines $(Mg,Fe)_3Si_2O_5(OH)_4$, ...
  - nonporous ice/water
- density in each layer ~ constant (neglect of compression effects)

$$M = \frac{4}{3}\pi\rho R^3 = M_r + M_i = \rho_r V_r + \rho_i V_i = \frac{4}{3}\pi\left[\rho_r R_r^3 + \rho_i\left(R^3 - R_r^3\right)\right]$$

$$\rho R^3 = \rho_r R_r^3 + \rho_i\left(R^3 - R_r^3\right)$$

- water/ice density ρ_i~1000 kg m^{-3} (well constrained)
- rock density ρ_r~2500 (hydrated rock) – 8000 kg m^{-3} (pure iron)
- nonhydrated rock ρ_r~3500 kg m^{-3} (close to ρ_{Io})

Average density and ice mass fraction

(*Hussmann* +, 2015)

- main composition (~abundances of outer solar system nebula)
  - rock (including iron): olivine $(Mg^{2+},Fe^{2+})_2SiO_4$, pyroxenes $XY(Si,Al)_2O_6$, serpentines $(Mg,Fe)_3Si_2O_5(OH)_4$, ...
  - nonporous ice/water
- density in each layer ~ constant (neglect of compression effects)

$$M = \frac{4}{3}\pi\rho R^3 = M_r + M_i = \rho_r V_r + \rho_i V_i = \frac{4}{3}\pi\left[\rho_r R_r^3 + \rho_i\left(R^3 - R_r^3\right)\right]$$

$$\rho R^3 = \rho_r R_r^3 + \rho_i\left(R^3 - R_r^3\right)$$

- water/ice density ρ_i~1000 kg m^{-3} (well constrained)
- rock density ρ_r~2500 (hydrated rock) – 8000 kg m^{-3} (pure iron)
- nonhydrated rock ρ_r~3500 kg m^{-3} (close to ρ_{Io})

$$R_r = R\left(\frac{\rho - \rho_i}{\rho_r - \rho_i}\right)^{1/3}$$

- rock and ice mass fractions can be determined from the density

Average density and ice mass fraction

(*Hussmann* +, 2015; *Iess* +, 2014; *Durante* +, 2019)

- assuming complete differentiation into a rock core and an icy mantle

	Europa	Ganymede	Enceladus	Titan
M [10^{22} kg]	4.8	14.8	0.01	13.5
R [km]	1565	2631	252	2575

Average density and ice mass fraction

(*Hussmann* +, 2015; *Iess* +, 2014; *Durante* +, 2019)

- assuming complete differentiation into a rock core and an icy mantle
- $\rho = \frac{3M}{4\pi R^3}$

	Europa	Ganymede	Enceladus	Titan
M [10^{22} kg]	4.8	14.8	0.01	13.5
R [km]	1565	2631	252	2575
ρ [kg m^{-3}]	2990	1940	1492	1888

Average density and ice mass fraction

(*Hussmann* +, 2015; *Iess* +, 2014; *Durante* +, 2019)

- assuming complete differentiation into a rock core and an icy mantle
- $\rho = \frac{3M}{4\pi R^3}$
- $\rho_r \sim 3500$, $\rho_i \sim 1000$: $R_r = R\left(\frac{\rho-\rho_i}{\rho_r-\rho_i}\right)^{1/3}$

	Europa	Ganymede	Enceladus	Titan
M [10^{22} kg]	4.8	14.8	0.01	13.5
R [km]	1565	2631	252	2575
ρ [kg m^{-3}]	2990	1940	1492	1888
R_r [km]	1450	1899	147	1823

Average density and ice mass fraction

(*Hussmann* +, 2015; *Iess* +, 2014; *Durante* +, 2019)

- assuming complete differentiation into a rock core and an icy mantle
- $\rho = \frac{3M}{4\pi R^3}$
- ρ_r~3500, ρ_i~1000: $R_r = R\left(\frac{\rho-\rho_i}{\rho_r-\rho_i}\right)^{1/3}$
- $d_i = R - R_r$

	Europa	Ganymede	Enceladus	Titan
M [10^{22} kg]	4.8	14.8	0.01	13.5
R [km]	1565	2631	252	2575
ρ [kg m^{-3}]	2990	1940	1492	1888
R_r [km]	1450	1899	147	1823
d_i [km]	115	732	105	752

Average density and ice mass fraction

(*Hussmann* +, 2015; *Iess* +, 2014; *Durante* +, 2019)

- assuming complete differentiation into a rock core and an icy mantle
- $\rho = \frac{3M}{4\pi R^3}$
- $\rho_r \sim 3500$, $\rho_i \sim 1000$: $R_r = R\left(\frac{\rho - \rho_i}{\rho_r - \rho_i}\right)^{1/3}$
- $d_i = R - R_r$
- $M_i = \frac{4}{3}\pi\rho_i(R^3 - R_r^3)$, $m_i = \frac{M_i}{M}$

	Europa	Ganymede	Enceladus	Titan
M [10^{22} kg]	4.8	14.8	0.01	13.5
R [km]	1565	2631	252	2575
ρ [kg m^{-3}]	2990	1940	1492	1888
R_r [km]	1450	1899	147	1823
d_i [km]	115	732	105	752
M_i [10^{22} kg]	0.3278	4.7602	0.0054	4.6126
m_i [%]	7	32	54	34

Average density and ice mass fraction

(*Hussmann* +, 2015)

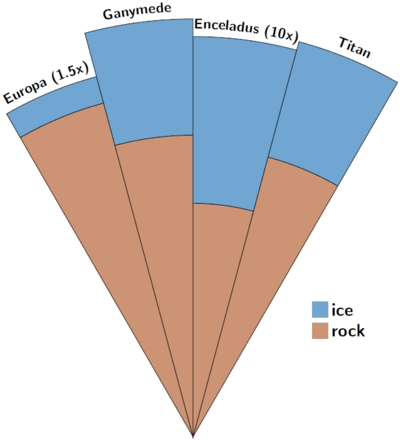

- degree of differentiation (complete or homogeneous ice-rock mixture) has to be inferred from spacecraft flybys

Hydrostatic equilibrium and satellite shape

(*Schubert* +, 2009; *Hemingway* +, 2018)

- interior of large planetary bodies: high pressures + low viscosities

→ relaxation to hydrostatic shape = shape of strengthless fluid body (inward gravity acceleration balanced by fluid pressure gradient):

$$dP = -\rho(r)g(r)dr$$

Hydrostatic equilibrium and satellite shape

(*Schubert* +, 2009; *Hemingway* +, 2018)

- interior of large planetary bodies: high pressures + low viscosities

→ relaxation to hydrostatic shape = shape of strengthless fluid body (inward gravity acceleration balanced by fluid pressure gradient):

$$dP = -\rho(r)g(r)dr$$

- hydrostatic shape:

- selfgravitation alone: sphere
- rotation: centrifugal flattening
- synchronous rotation with parent body (tidal locking): permanent elongation along the tidal axis

Hydrostatic equilibrium and satellite shape

(*Schubert* +, 2009; *Hemingway* +, 2018)

- interior of large planetary bodies: high pressures + low viscosities

→ relaxation to hydrostatic shape = shape of strengthless fluid body (inward gravity acceleration balanced by fluid pressure gradient):

$$dP = -\rho(r)g(r)dr$$

- hydrostatic shape:
  - selfgravitation alone: sphere
  - rotation: centrifugal flattening
  - synchronous rotation with parent body (tidal locking): permanent elongation along the tidal axis
- tidal + rotational deformation → satellites relax to a 3-axial ellipsoid ($a > b > c$)

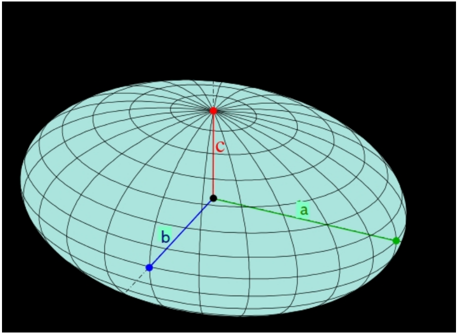

Hydrostatic equilibrium and satellite shape

(*Schubert* +, 2009; *Hemingway* +, 2018)

- satellite shape can provide additional clues on the interior structure
- accurate measurements of shape can provide evidence for (or against) the hydrostatic state obtained by the satellite

$$\frac{b-c}{a-c} = \frac{1}{4}$$

Hydrostatic equilibrium and satellite shape

(*Schubert* +, 2009; *Hemingway* +, 2018)

- satellite shape can provide additional clues on the interior structure
- accurate measurements of shape can provide evidence for (or against) the hydrostatic state obtained by the satellite

$$\frac{b-c}{a-c} = \frac{1}{4}$$

- deviations from hydrostatic state e.g. due to internal activity, incomplete relaxation, 'frozen in' structure, ...

Hydrostatic equilibrium and satellite shape

(*Schubert* +, 2009; *Hemingway* +, 2018)

- satellite shape can provide additional clues on the interior structure
- accurate measurements of shape can provide evidence for (or against) the hydrostatic state obtained by the satellite

$$\frac{b-c}{a-c} = \frac{1}{4}$$

- deviations from hydrostatic state e.g. due to internal activity, incomplete relaxation, 'frozen in' structure, ...
- hydrostatic shape → hydrostatic gravitational field
- nonhydrostatic shape + hydrostatic gravity field → compensation: gravity anomaly due to shape reduced by internal density anomaly

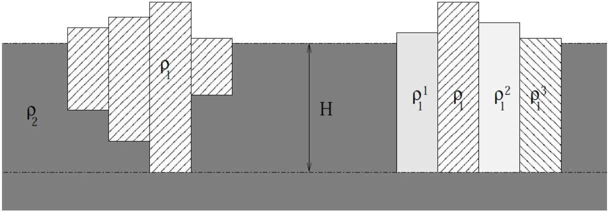

Gravitational potential

- Newton integral

$$
\begin{aligned}
V(r,\theta,\phi) &= G\int_{\Omega}\frac{dm(r',\theta',\phi')}{|\vec{r}-\vec{r'}|} \\
&= G\int_0^R\int_0^{\pi}\int_0^{2\pi}\frac{\rho(r',\theta',\phi')}{|\vec{r}-\vec{r'}|}(r')^2\sin\theta' dr' d\theta' d\phi'
\end{aligned}
$$

Gravitational potential

- Newton integral

$$V(r,\theta,\phi) = G\int_\Omega \frac{dm(r',\theta',\phi')}{|\vec{r}-\vec{r'}|}$$
$$= G\int_0^R\int_0^\pi\int_0^{2\pi}\frac{\rho(r',\theta',\phi')}{|\vec{r}-\vec{r'}|}(r')^2\sin\theta' dr' d\theta' d\phi'$$

- expansion into series of spherical harmonic functions

$$V(r,\theta,\phi) = \frac{GM}{r}\sum_{j=0}^{\infty}\left(\frac{R}{r}\right)^j\sum_{m=0}^{j}P_{jm}(\cos\theta)\Big[C_{jm}\cos m\phi + S_{jm}\sin m\phi\Big]$$

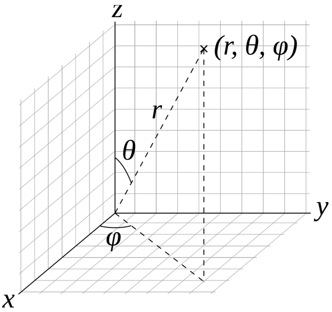

Gravitational potential

- Newton integral

$$V(r,\theta,\phi) = G\int_\Omega \frac{dm(r',\theta',\phi')}{|\vec{r}-\vec{r'}|}$$
$$= G\int_0^R\int_0^\pi\int_0^{2\pi} \frac{\rho(r',\theta',\phi')}{|\vec{r}-\vec{r'}|}(r')^2\sin\theta' dr' d\theta' d\phi'$$

- expansion into series of spherical harmonic functions

$$V(r,\theta,\phi) = \frac{GM}{r}\sum_{j=0}^{\infty}\left(\frac{R}{r}\right)^j\sum_{m=0}^{j}P_{jm}(\cos\theta)\Big[C_{jm}\cos m\phi + S_{jm}\sin m\phi\Big]$$

- $P_{jm}(\xi)$: associated Legendre functions:
  $P_{jm}(\xi) = (1-\xi^2)^{m/2}\frac{d^m}{d\xi^m}P_j(\xi)$

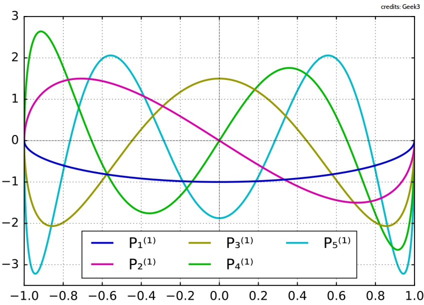

Gravitational potential

- Newton integral

$$V(r,\theta,\phi) = G\int_\Omega \frac{dm(r',\theta',\phi')}{|\vec{r}-\vec{r'}|}$$

$$= G\int_0^R\int_0^\pi\int_0^{2\pi} \frac{\rho(r',\theta',\phi')}{|\vec{r}-\vec{r'}|}(r')^2\sin\theta' dr' d\theta' d\phi'$$

- expansion into series of spherical harmonic functions

$$V(r,\theta,\phi) = \frac{GM}{r}\sum_{j=0}^{\infty}\left(\frac{R}{r}\right)^j \sum_{m=0}^{j} P_{jm}(\cos\theta)\Big[C_{jm}\cos m\phi + S_{jm}\sin m\phi\Big]$$

- $P_{jm}(\xi)$: associated Legendre functions: $P_{jm}(\xi) = (1-\xi^2)^{m/2}\frac{d^m}{d\xi^m}P_j(\xi)$
- $P_j(\xi)$: Legendre polynoms: $P_j(\xi) = \frac{1}{2^j j!}\frac{d^j}{d\xi^j}(\xi^2-1)^j$

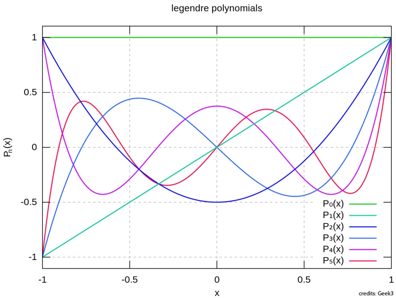

Gravitational potential

- Newton integral

$$V(r,\theta,\phi) = G\int_\Omega \frac{dm(r',\theta',\phi')}{|\vec{r}-\vec{r'}|}$$
$$= G\int_0^R\int_0^\pi\int_0^{2\pi} \frac{\rho(r',\theta',\phi')}{|\vec{r}-\vec{r'}|}(r')^2\sin\theta' dr' d\theta' d\phi'$$

- expansion into series of spherical harmonic functions

$$V(r,\theta,\phi) = \frac{GM}{r}\sum_{j=0}^{\infty}\left(\frac{R}{r}\right)^j \sum_{m=0}^{j} P_{jm}(\cos\theta)\Big[C_{jm}\cos m\phi + S_{jm}\sin m\phi\Big]$$

- $P_{jm}(\xi)$: associated Legendre functions: $P_{jm}(\xi) = (1-\xi^2)^{m/2}\frac{d^m}{d\xi^m}P_j(\xi)$
- $P_j(\xi)$: Legendre polynoms: $P_j(\xi) = \frac{1}{2^j j!}\frac{d^j}{d\xi^j}(\xi^2-1)^j$
- C_{jm}, S_{jm}: harmonic coefficients (j degree, m order); note $S_{j0} = 0 \quad \forall j$

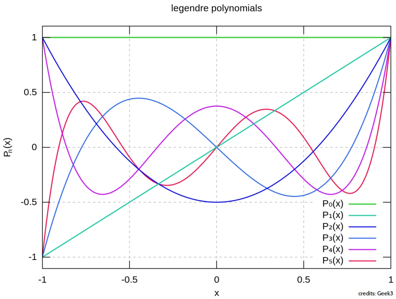

Harmonic coefficients - meaning

$$V(r,\theta,\phi) = \frac{GM}{r}\sum_{j=0}^{\infty}\left(\frac{R}{r}\right)^j \sum_{m=0}^{j} P_{jm}(\cos\theta)\Big[C_{jm}\cos m\phi + S_{jm}\sin m\phi\Big]$$

Harmonic coefficients - meaning

$$V(r,\theta,\phi) = \frac{GM}{r}\sum_{j=0}^{\infty}\left(\frac{R}{r}\right)^{j}\sum_{m=0}^{j}P_{jm}(\cos\theta)\Big[C_{jm}\cos m\phi + S_{jm}\sin m\phi\Big]$$

$j = 0$ potential of point of mass M in the origin of coordinate system:
$C_{00} = 1,\ S_{00} = 0$

Harmonic coefficients - meaning

$$V(r,\theta,\phi) = \frac{GM}{r}\sum_{j=0}^{\infty}\left(\frac{R}{r}\right)^j \sum_{m=0}^{j} P_{jm}(\cos\theta)\left[C_{jm}\cos m\phi + S_{jm}\sin m\phi\right]$$

$j = 0$ potential of point of mass M in the origin of coordinate system:
$C_{00} = 1,\ S_{00} = 0$

$j = 1$ position of center of mass wrt to the origin:
$C_{11} = \frac{x}{R},\ S_{11} = \frac{y}{R},\ C_{10} = \frac{z}{R}$
specially choose: origin in the center of mass
$\rightarrow C_{11} = S_{11} = C_{10} = 0$

Harmonic coefficients - meaning

$$V(r,\theta,\phi) = \frac{GM}{r}\sum_{j=0}^{\infty}\left(\frac{R}{r}\right)^{j}\sum_{m=0}^{j}P_{jm}(\cos\theta)\Big[C_{jm}\cos m\phi + S_{jm}\sin m\phi\Big]$$

$j = 0$ potential of point of mass M in the origin of coordinate system:
$C_{00} = 1,\ S_{00} = 0$

$j = 1$ position of center of mass wrt to the origin:
$C_{11} = \frac{x}{R},\ S_{11} = \frac{y}{R},\ C_{10} = \frac{z}{R}$
specially choose: origin in the center of mass
$\rightarrow C_{11} = S_{11} = C_{10} = 0$

$j = 2$ components of the moment of inertia tensor $\boldsymbol{I}$:

$$C_{20} = -\frac{1}{MR^2}\left[I_{zz} - \frac{I_{xx} + I_{yy}}{2}\right]$$

$$C_{21} = \frac{I_{xz}}{MR^2},\quad S_{21} = \frac{I_{yz}}{MR^2}$$

$$C_{22} = -\frac{1}{4MR^2}\left(I_{xx} - I_{yy}\right),\quad S_{22} = \frac{I_{xy}}{MR^2}$$

specially choose: coordinate axes = principal axes of $\boldsymbol{I}$
$\rightarrow C_{21} = S_{21} = S_{22} = 0$

Synchronously rotating satellite in hydrostatic equilibrium

(*Schubert* +, 2009; *Hemingway* +, 2018)

$$C_{20} = -\frac{1}{MR^2}\left[I_{zz} - \frac{I_{xx} + I_{yy}}{2}\right], \quad C_{22} = -\frac{1}{4MR^2}\left(I_{xx} - I_{yy}\right)$$

Synchronously rotating satellite in hydrostatic equilibrium

(*Schubert* +, 2009; *Hemingway* +, 2018)

$$C_{20} = -\frac{1}{MR^2}\left[I_{zz} - \frac{I_{xx} + I_{yy}}{2}\right], \quad C_{22} = -\frac{1}{4MR^2}\left(I_{xx} - I_{yy}\right)$$

- principal moments of inertia: $C > B > A$
- $C = I_{zz}, \ B = I_{yy}, \ A = I_{xx}$

Synchronously rotating satellite in hydrostatic equilibrium

(*Schubert* +, 2009; *Hemingway* +, 2018)

$$C_{20} = -\frac{1}{MR^2}\left[I_{zz} - \frac{I_{xx} + I_{yy}}{2}\right], \quad C_{22} = -\frac{1}{4MR^2}\left(I_{xx} - I_{yy}\right)$$

- principal moments of inertia: $C > B > A$
- $C = I_{zz},\ B = I_{yy},\ A = I_{xx}$
- dynamical polar flattening J_2:

$$J_2 = -C_{20} = \frac{1}{MR^2}\left[C - \frac{A+B}{2}\right]$$

- mainly caused by satellite's rotation
- best determined with a polar flyby

Synchronously rotating satellite in hydrostatic equilibrium

(*Schubert* +, 2009; *Hemingway* +, 2018)

$$C_{20} = -\frac{1}{MR^2}\left[I_{zz} - \frac{I_{xx} + I_{yy}}{2}\right], \quad C_{22} = -\frac{1}{4MR^2}\left(I_{xx} - I_{yy}\right)$$

- principal moments of inertia: $C > B > A$
- $C = I_{zz},\ B = I_{yy},\ A = I_{xx}$
- dynamical polar flattening J_2:

$$J_2 = -C_{20} = \frac{1}{MR^2}\left[C - \frac{A+B}{2}\right]$$

- mainly caused by satellite's rotation
- best determined with a polar flyby

- equatorial bulge C_{22}:

$$C_{22} = \frac{1}{4MR^2}\left(B - A\right)$$

- pointing toward the primary due to tidal interaction
- best determined by equatorial flyby

Tidal & rotational disturbing potential

(*Schubert* +, 2009; *Hemingway* +, 2018)

- tidal & rotational forces:

→ deviation from spherical symmetry

→ disturbances in the potential field

Tidal & rotational disturbing potential

(*Schubert* +, 2009; *Hemingway* +, 2018)

- tidal & rotational forces:

→ deviation from spherical symmetry

→ disturbances in the potential field

- centrifugal disturbing potential at the surface:

$$V_r(\theta, \phi) \sim \frac{1}{3}\omega^2 R^2 P_{20}(\cos\theta)$$

Tidal & rotational disturbing potential

(*Schubert* +, 2009; *Hemingway* +, 2018)

- tidal & rotational forces:

→ deviation from spherical symmetry

→ disturbances in the potential field

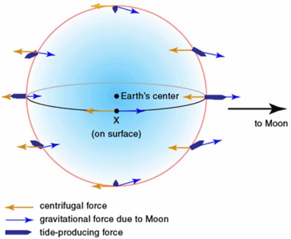

- centrifugal disturbing potential at the surface:

$$V_r(\theta,\phi) \sim \frac{1}{3}\omega^2 R^2 P_{20}(\cos\theta)$$

- tidal disturbing potential (neglecting terms $\sim e$)

$$V_t(\theta,\phi) \sim \frac{GM_p R^2}{a_p^3}\left[\frac{1}{2}P_{20}(\cos\theta) - \frac{1}{4}P_{22}(\cos\theta)\cos(2\phi)\right]$$

(a_p distance to tide-raising body, M_p its mass)

Tidal & rotational disturbing potential

(*Schubert* +, 2009; *Hemingway* +, 2018)

- rotation coefficient q_r (deformation due to rotation)

- equatorial centrigual potential vs gravitational potential at surface
- symmetry axis: the polar (z) axis

$$q_r = \frac{\omega^2 R^2}{GM/R} = \frac{\omega^2 R^3}{GM}$$

Tidal & rotational disturbing potential

(*Schubert* +, 2009; *Hemingway* +, 2018)

- rotation coefficient q_r (deformation due to rotation)
- equatorial centrigual potential vs gravitational potential at surface
- symmetry axis: the polar (z) axis

$$q_r = \frac{\omega^2 R^2}{GM/R} = \frac{\omega^2 R^3}{GM}$$

- tidal coefficient q_t (deformation due to tides):
- surface tidal potential vs gravitational potential at surface
- symmetry axis: the sub-primary line (x axis)

$$q_t = -3\frac{GM_p R^2/(a_p)^3}{GM/R} = -3\left(\frac{R}{a_p}\right)^3 \frac{M_p}{M}$$

Synchronously rotating satellite in hydrostatic equilibrium

(*Schubert* +, 2009; *Hemingway* +, 2018)

- Kepler's 3rd law:

$$\frac{(a_p)^3}{T^2} = \frac{(a_p)^3 n^2}{4\pi^2} = \frac{G(M_p + M)}{4\pi^2} \sim \frac{GM_p}{4\pi^2}$$

Synchronously rotating satellite in hydrostatic equilibrium

(*Schubert* +, 2009; *Hemingway* +, 2018)

- Kepler's 3rd law:

$$\frac{(a_p)^3}{T^2} = \frac{(a_p)^3 n^2}{4\pi^2} = \frac{G(M_p + M)}{4\pi^2} \sim \frac{GM_p}{4\pi^2}$$

- synchronous rotation: $n = \omega \rightarrow (a_p)^3 = \frac{GM_p}{\omega^2}$

Synchronously rotating satellite in hydrostatic equilibrium

(*Schubert* +, 2009; *Hemingway* +, 2018)

- Kepler's 3rd law:

$$\frac{(a_p)^3}{T^2} = \frac{(a_p)^3 n^2}{4\pi^2} = \frac{G(M_p + M)}{4\pi^2} \sim \frac{GM_p}{4\pi^2}$$

- synchronous rotation: $n = \omega \to (a_p)^3 = \frac{GM_p}{\omega^2}$

$$q_t = -3\left(\frac{R}{a_p}\right)^3 \frac{M_p}{M} = -3\frac{R^3\omega^2}{GM_p}\frac{M_p}{M} = -3\frac{R^3\omega^2}{GM} = -3q_r$$

- magnitudes of rotational and tidal deformation differ by a factor of 3
- opposite sign: flattening vs bulge

Synchronously rotating satellite in hydrostatic equilibrium

(*Schubert* +, 2009; *Hemingway* +, 2018)

- Kepler's 3rd law:

$$\frac{(a_p)^3}{T^2} = \frac{(a_p)^3 n^2}{4\pi^2} = \frac{G(M_p + M)}{4\pi^2} \sim \frac{GM_p}{4\pi^2}$$

- synchronous rotation: $n = \omega \rightarrow (a_p)^3 = \frac{GM_p}{\omega^2}$

$$q_t = -3\left(\frac{R}{a_p}\right)^3 \frac{M_p}{M} = -3\frac{R^3\omega^2}{GM_p}\frac{M_p}{M} = -3\frac{R^3\omega^2}{GM} = -3q_r$$

- magnitudes of rotational and tidal deformation differ by a factor of 3
- opposite sign: flattening vs bulge

	Europa	Ganymede	Enceladus	Titan
R [km]	1565	2631	252	2575
ω [10^{-5} s^{-1}]	2.0	1.0	5.3	0.5
GM [10^3 km^3 s^{-2}]	3.2	9.9	6.7	9.0
q_r [10^{-4}]	5.0	1.9	67.5	0.4
q_t [10^{-4}]	−15.0	−5.7	−202.5	−1.2

Synchronously rotating satellite in hydrostatic equilibrium

(*Schubert* +, 2009; *Hemingway* +, 2018)

- Kepler's 3rd law:

$$\frac{(a_p)^3}{T^2} = \frac{(a_p)^3 n^2}{4\pi^2} = \frac{G(M_p + M)}{4\pi^2} \sim \frac{GM_p}{4\pi^2}$$

- synchronous rotation: $n = \omega \to (a_p)^3 = \frac{GM_p}{\omega^2}$

$$q_t = -3\left(\frac{R}{a_p}\right)^3 \frac{M_p}{M} = -3\frac{R^3\omega^2}{GM_p}\frac{M_p}{M} = -3\frac{R^3\omega^2}{GM} = -3q_r$$

- magnitudes of rotational and tidal deformation differ by a factor of 3
- opposite sign: flattening vs bulge

	Europa	Ganymede	Enceladus	Titan	
R [km]	1565	2631	252	2575	
ω [10^{-5} s^{-1}]	2.0	1.0	5.3	0.5	
GM [10^3 km^3 s^{-2}]	3.2	9.9	6.7	9.0	
q_r [10^{-4}]	5.0	1.9	67.5	0.4	
q_t [10^{-4}]	−15.0	−5.7	−202.5	−1.2	$\ll 1$

Synchronously rotating satellite in hydrostatic equilibrium

(*Hubbard & Anderson*, 1978)

- $q_r,\, q_t \ll 1 \rightarrow$ first-order theory of figures:

$$J_2 = \frac{1}{3} k_f \left(q_r - \frac{1}{2} q_t \right), \quad C_{22} = -\frac{1}{12} k_f q_t$$

Synchronously rotating satellite in hydrostatic equilibrium
(*Hubbard & Anderson*, 1978)

- $q_r,\, q_t \ll 1 \rightarrow$ first-order theory of figures:

$$J_2 = \frac{1}{3} k_f \left(q_r - \frac{1}{2} q_t \right), \quad C_{22} = -\frac{1}{12} k_f q_t$$

- fluid Love number k_f:
- depends on distribution of mass within the satellite
- $k_f = \frac{3}{2}$ for constant density

Synchronously rotating satellite in hydrostatic equilibrium

(*Hubbard & Anderson*, 1978)

- $q_r,\, q_t \ll 1 \rightarrow$ first-order theory of figures:

$$J_2 = \frac{1}{3} k_f \left(q_r - \frac{1}{2} q_t \right), \quad C_{22} = -\frac{1}{12} k_f q_t$$

- fluid Love number k_f:
- depends on distribution of mass within the satellite
- $k_f = \frac{3}{2}$ for constant density
- synchronously rotating satellite ($q_t = -3q_r$)

$$J_2 = \frac{5}{6} k_f q_r, \quad C_{22} = \frac{1}{4} k_f q_r$$

Synchronously rotating satellite in hydrostatic equilibrium

(*Hubbard & Anderson*, 1978)

- $q_r,\, q_t \ll 1 \rightarrow$ first-order theory of figures:

$$J_2 = \frac{1}{3} k_f \left(q_r - \frac{1}{2} q_t \right), \quad C_{22} = -\frac{1}{12} k_f q_t$$

- fluid Love number k_f:
- depends on distribution of mass within the satellite
- $k_f = \frac{3}{2}$ for constant density
- synchronously rotating satellite ($q_t = -3q_r$)

$$J_2 = \frac{5}{6} k_f q_r, \quad C_{22} = \frac{1}{4} k_f q_r$$

- relation between gravity coefficients

$$\boxed{J_2 = \frac{10}{3} C_{22}}$$

Determining J_2, C_{22}

(*Schubert* +, 2009)

- determination of coefficients C_{jm} and S_{jm} from Doppler data
- number of independent coefs $\propto$ number of flybys & geometry:
- the best configuration: spacecraft in polar orbit
- several flybys / orbiter $\rightarrow$ J_2 and C_{22} can be inferred independently

Determining J_2, C_{22}

($\mathit{Schubert}$ +, 2009)

- determination of coefficients C_{jm} and S_{jm} from Doppler data
- number of independent coefs $\propto$ number of flybys & geometry:
- the best configuration: spacecraft in polar orbit
- several flybys / orbiter $\rightarrow$ J_2 and C_{22} can be inferred independently

Galileo 2 or at most a few flybys $\rightarrow$ J_2 and C_{22} are not independent

$\rightarrow$ hydrostatic equilibrium used as a reasonable first order estimate

$\rightarrow$ $J_2 = \frac{10}{3} C_{22}$ imposed to determine J_2 and C_{22} from Doppler data

Determining J_2, C_{22}

(*Schubert* +, 2009)

- determination of coefficients C_{jm} and S_{jm} from Doppler data
- number of independent coefs $\propto$ number of flybys & geometry:

- the best configuration: spacecraft in polar orbit
- several flybys / orbiter $\rightarrow$ J_2 and C_{22} can be inferred independently

Galileo 2 or at most a few flybys $\rightarrow$ J_2 and C_{22} are not independent

$\rightarrow$ hydrostatic equilibrium used as a reasonable first order estimate

$\rightarrow$ $J_2 = \frac{10}{3} C_{22}$ imposed to determine J_2 and C_{22} from Doppler data

Cassini J_2 and C_{22} determined nearly independently, their ratio close to hydrostatic equilibrium (*Iess* +, 2014; *Durante* +, 2019)

Determining J_2, C_{22}

(*Schubert* +, 2009)

- determination of coefficients C_{jm} and S_{jm} from Doppler data
- number of independent coefs $\propto$ number of flybys & geometry:
- the best configuration: spacecraft in polar orbit
- several flybys / orbiter $\rightarrow$ J_2 and C_{22} can be inferred independently

Galileo 2 or at most a few flybys $\rightarrow$ J_2 and C_{22} are not independent

$\rightarrow$ hydrostatic equilibrium used as a reasonable first order estimate

$\rightarrow$ $J_2 = \frac{10}{3} C_{22}$ imposed to determine J_2 and C_{22} from Doppler data

Cassini J_2 and C_{22} determined nearly independently, their ratio close to hydrostatic equilibrium (*Iess* +, 2014; *Durante* +, 2019)

- Doppler $\rightarrow$ C_{22} $\rightarrow$ $k_f = \frac{4C_{22}}{q_r}$

Determining J_2, C_{22}, and C

(*Schubert* +, 2009)

- determination of coefficients C_{jm} and S_{jm} from Doppler data
- number of independent coefs $\propto$ number of flybys & geometry:
- \- the best configuration: spacecraft in polar orbit
- \- several flybys / orbiter $\rightarrow$ J_2 and C_{22} can be inferred independently

Galileo 2 or at most a few flybys $\rightarrow$ J_2 and C_{22} are not independent

$\rightarrow$ hydrostatic equilibrium used as a reasonable first order estimate

$\rightarrow$ $J_2 = \frac{10}{3} C_{22}$ imposed to determine J_2 and C_{22} from Doppler data

Cassini J_2 and C_{22} determined nearly independently, their ratio close to hydrostatic equilibrium (*Iess* +, 2014; *Durante* +, 2019)

- Doppler $\rightarrow$ C_{22} $\rightarrow$ $k_f = \frac{4C_{22}}{q_r}$ $\rightarrow$ polar moment of inertia C
- Radau-Darwin equation:

$$\boxed{\frac{C}{MR^2} = \frac{2}{3}\left[1 - \frac{2}{5}\left(\frac{4-k_f}{1+k_f}\right)^{1/2}\right]}$$

Two/three-layered models

- core (ρ_c=ρ_m, R_c=R_m), hydrosphere / core, mantle, hydrosphere

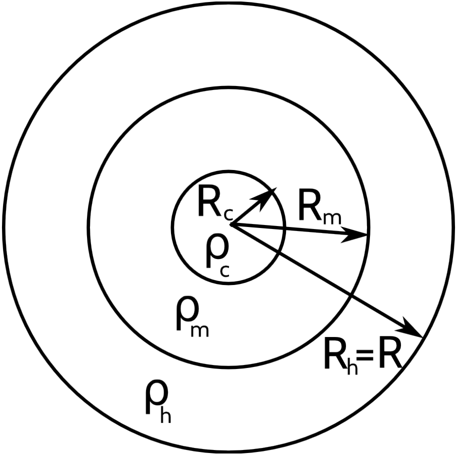

Two/three-layered models

- core (ρ_c=ρ_m, R_c=R_m), hydrosphere / core, mantle, hydrosphere
- mass

$$M = M_c + M_m + M_h = \frac{4}{3}\pi\left[\rho_c R_c^3 + \rho_m(R_m^3 - R_c^3) + \rho_h(R^3 - R_m^3)\right]$$

Two/three-layered models

- core (ρ_c=ρ_m, R_c=R_m), hydrosphere / core, mantle, hydrosphere
- mass

$$M = M_c + M_m + M_h = \frac{4}{3}\pi\left[\rho_c R_c^3 + \rho_m(R_m^3 - R_c^3) + \rho_h(R^3 - R_m^3)\right]$$

- polar moment of inertia

$$\begin{aligned} C &= \int_\Omega \rho(x^2 + y^2)d\Omega = \int_0^R \int_0^\pi \int_0^{2\pi} \rho(r)r^2 \sin\theta^2 r^2 \sin\theta dr d\theta d\phi \\ &= \frac{8\pi}{3}\int_0^R \rho(r)r^4 dr = \frac{8\pi}{15}\left[\rho_c R_c^5 + \rho_m(R_m^5 - R_c^5) + \rho_h(R^5 - R_m^5)\right] \end{aligned}$$

Two/three-layered models

- core (ρ_c=ρ_m, R_c=R_m), hydrosphere / core, mantle, hydrosphere
- mass

$$M = M_c + M_m + M_h = \frac{4}{3}\pi\left[\rho_c R_c^3 + \rho_m (R_m^3 - R_c^3) + \rho_h (R^3 - R_m^3)\right]$$

- polar moment of inertia

$$C = \int_\Omega \rho(x^2 + y^2) d\Omega = \int_0^R \int_0^\pi \int_0^{2\pi} \rho(r) r^2 \sin\theta^2 r^2 \sin\theta dr d\theta d\phi$$
$$= \frac{8\pi}{3} \int_0^R \rho(r) r^4 dr = \frac{8\pi}{15}\left[\rho_c R_c^5 + \rho_m (R_m^5 - R_c^5) + \rho_h (R^5 - R_m^5)\right]$$

- reduced moment of inertia (MoI)

$$\mathrm{MoI} = \frac{C}{MR^2} = \frac{3C}{4\pi\rho R^5} = \frac{2}{5}\frac{1}{\rho R^5}\left[\rho_c R_c^5 + \rho_m (R_m^5 - R_c^5) + \rho_h (R^5 - R_m^5)\right]$$

Two/three-layered models

- core (ρ_c=ρ_m, R_c=R_m), hydrosphere / core, mantle, hydrosphere
- mass

$$M = M_c + M_m + M_h = \frac{4}{3}\pi\left[\rho_c R_c^3 + \rho_m(R_m^3 - R_c^3) + \rho_h(R^3 - R_m^3)\right]$$

- polar moment of inertia

$$C = \int_\Omega \rho(x^2 + y^2)d\Omega = \int_0^R \int_0^\pi \int_0^{2\pi} \rho(r) r^2 \sin\theta^2 r^2 \sin\theta dr d\theta d\phi$$
$$= \frac{8\pi}{3}\int_0^R \rho(r) r^4 dr = \frac{8\pi}{15}\left[\rho_c R_c^5 + \rho_m(R_m^5 - R_c^5) + \rho_h(R^5 - R_m^5)\right]$$

- reduced moment of inertia (MoI)

$$\mathrm{MoI} = \frac{C}{MR^2} = \frac{3C}{4\pi\rho R^5} = \frac{2}{5}\frac{1}{\rho R^5}\left[\rho_c R_c^5 + \rho_m(R_m^5 - R_c^5) + \rho_h(R^5 - R_m^5)\right]$$

- constant density ($\rho_c = \rho_m = \rho_h = \rho$): $\mathrm{MoI} = \frac{2}{5}$
- $\mathrm{MoI} < \frac{2}{5}$: increase of density with depth (differentiation)

Two/three-layered models

- two-layered models:
- data: M, C
- 3 unknown parameters: R_c, ρ_c, ρ_h

Two/three-layered models

- two-layered models:
- data: M, C
- 3 unknown parameters: R_c, ρ_c, ρ_h

(a) 1 parameter needs to be fixed (e.g. ρ_h)
2 other parameters are computed (R_c, ρ_c)

Two/three-layered models

- two-layered models:
- data: M, C
- 3 unknown parameters: R_c, ρ_c, ρ_h

(a) 1 parameter needs to be fixed (e.g. ρ_h)
2 other parameters are computed (R_c, ρ_c)

(b) forward modeling: set of possible models that satisfy data

Two/three-layered models

- two-layered models:
  - data: M, C
  - 3 unknown parameters: R_c, ρ_c, ρ_h

  (a) 1 parameter needs to be fixed (e.g. ρ_h)
  2 other parameters are computed (R_c, ρ_c)

  (b) forward modeling: set of possible models that satisfy data

- three-layered models:
  - data: M, C
  - 5 unknown parameters: R_c, ρ_c, R_m, ρ_m, ρ_h

Two/three-layered models

- two-layered models:
- data: M, C
- 3 unknown parameters: R_c, ρ_c, ρ_h

(a) 1 parameter needs to be fixed (e.g. ρ_h)
    2 other parameters are computed (R_c, ρ_c)
(b) forward modeling: set of possible models that satisfy data

- three-layered models:
- data: M, C
- 5 unknown parameters: R_c, ρ_c, R_m, ρ_m, ρ_h

(a) 3 parameters need to be chosen (e.g. ρ_c, ρ_m, ρ_h)
    2 other parameters are computed (R_c, R_m)
(b) forward modeling: set of possible models that satisfy data

Results of layered models: Europa

(*Anderson* +, 1998) - 4 gravity flybys

- $\mathrm{MoI} = 0.346 \rightarrow$ differentiated (mass concentration toward center)

Results of layered models: Europa

(*Anderson* +, 1998) - 4 gravity flybys

- $\mathrm{MoI} = 0.346 \rightarrow$ differentiated (mass concentration toward center)
- 2-layered models: $\rho_c > 3800$ kg m$^{-3} > \rho_{\mathrm{Io}}$

→ enrichment in dense metallic phases wrt Io by $\gtrsim$12%: unlikely

→ separation into metallic core and rock mantle more likely

Results of layered models: Europa

(*Anderson* +, 1998) - 4 gravity flybys

- $\mathrm{MoI} = 0.346 \rightarrow$ differentiated (mass concentration toward center)
- 2-layered models: $\rho_c > 3800$ kg m$^{-3} > \rho_{\mathrm{Io}}$

→ enrichment in dense metallic phases wrt Io by $\gtrsim$12%: unlikely

→ separation into metallic core and rock mantle more likely

- 3-layered models:

- R_c uncertain (Fe vs Fe-FeS), could be as large as ~$0.5R$
- silicate mantle
- hydrosphere thickness between 80 and 170 km

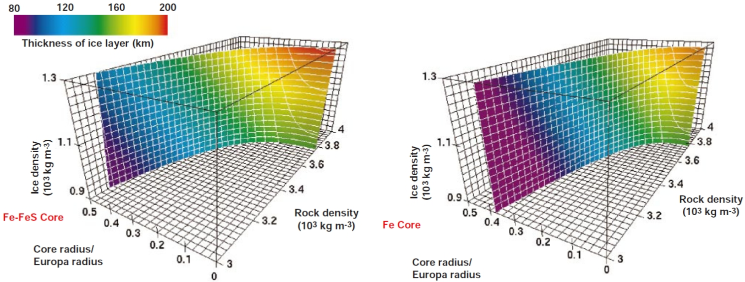

Results of layered models: Ganymede

(*Anderson* +, 1996) - 2 gravity flybys

- $\mathrm{MoI} = 0.3105$ → strongly differentiated
- among the smallest value in the Solar System (cf. Earth 0.334)
- average density → thick hydrosphere
- detected intrinsic magnetic field (*Kivelson* +, 1996) → metallic core

Results of layered models: Ganymede

(*Anderson* +, 1996) - 2 gravity flybys

- MoI = 0.3105 → strongly differentiated
- among the smallest value in the Solar System (cf. Earth 0.334)
- average density → thick hydrosphere
- detected intrinsic magnetic field (*Kivelson* +, 1996) → metallic core
- 3-layered models (more likely):
- metallic core of radius 400–1300 km (Fe vs Fe-FeS composition)
- silicate mantle
- hydrosphere ~800 km

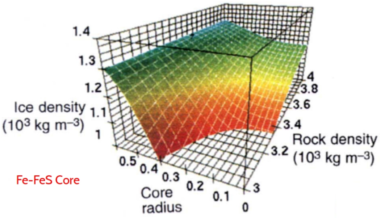

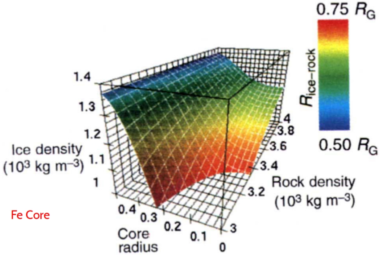

Results of layered models: Enceladus

(*Iess* +, 2014; *Hemingway* +, 2018) - 3 gravity flybys

- $\mathrm{MoI} = 0.335 \rightarrow$ mildly differentiated

Results of layered models: Enceladus

(*Iess* +, 2014; *Hemingway* +, 2018) - 3 gravity flybys

- $\mathrm{MoI} = 0.335 \rightarrow$ mildly differentiated
- Cassini: more precise, nearly independent measurements of J_2 & C_{22}
- $J_2/C_{22} = 3.51 > 10/3$: mild deviation from hydrostatic equilibrium

Results of layered models: Enceladus

(*Iess* +, 2014; *Hemingway* +, 2018) - 3 gravity flybys

- $\mathrm{MoI} = 0.335 \rightarrow$ mildly differentiated
- Cassini: more precise, nearly independent measurements of J_2 & C_{22}
- $J_2/C_{22} = 3.51 > 10/3$: mild deviation from hydrostatic equilibrium
- shape: $a - c = 6.00$ km, $b - c = 2.07$ km

$\rightarrow$ $(b - c)/(a - c) = 0.345 > 0.25$: considerable excess flattening

- nonhydrostatic contribution of shape to gravity small: compensation? ($\sim$ gravity anomaly associated with shape must be reduced by internal density anomaly)

Results of layered models: Enceladus

(*Iess* +, 2014; *Hemingway* +, 2018) - 3 gravity flybys

- $\mathrm{MoI} = 0.335 \rightarrow$ mildly differentiated
- Cassini: more precise, nearly independent measurements of J_2 & C_{22}
- $J_2/C_{22} = 3.51 > 10/3$: mild deviation from hydrostatic equilibrium
- shape: $a - c = 6.00$ km, $b - c = 2.07$ km

→ $(b - c)/(a - c) = 0.345 > 0.25$: considerable excess flattening

- nonhydrostatic contribution of shape to gravity small: compensation? (~ gravity anomaly associated with shape must be reduced by internal density anomaly)
- 2-layered models:

- low core density of ~2400 kg m^{-3}
- hydrosphere ~60 km
- compensation depth ~30–40 km: thickness of ice crust?
- negative mass anomaly in the South polar region - regional sea?

→ regional vs global ocean? cannot be answered with gravity data

Results of layered models: Titan

(*Durante* +, 2019) - 10 gravity flybys → coefficients up to degree 5

- MoI~0.341 → mildly differentiated

Results of layered models: Titan

(*Durante* +, 2019) - 10 gravity flybys → coefficients up to degree 5

- MoI~0.341 → mildly differentiated
- $J_2/C_{22} = 3.19 < 10/3$: mild deviation from hydrostatic equilibrium

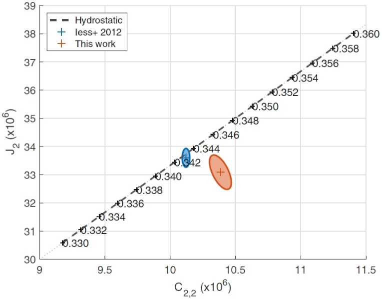

Results of layered models: Titan

(*Durante* +, 2019) - 10 gravity flybys → coefficients up to degree 5

- MoI~0.341 → mildly differentiated
- $J_2/C_{22} = 3.19 < 10/3$: mild deviation from hydrostatic equilibrium
- considerable excess flattening

→ the nonhydrostatic topography (> 500 m) must be compensated

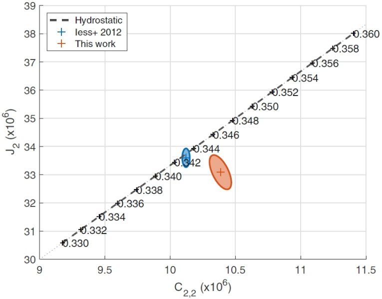

Results of layered models: Titan

(*Durante* +, 2019) - 10 gravity flybys → coefficients up to degree 5

- MoI~0.341 → mildly differentiated
- $J_2/C_{22} = 3.19 < 10/3$: mild deviation from hydrostatic equilibrium
- considerable excess flattening

→ the nonhydrostatic topography (> 500 m) must be compensated

- 2-layered models:

- if ρ_h~1000 kg m^{-3}: R_c~2200 km, ρ_c~2500 kg m^3, d_h~400 km
- if ρ_h larger and/or MoI smaller: smaller and denser cores

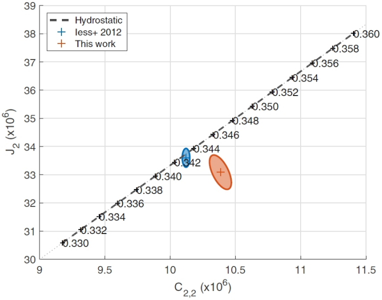

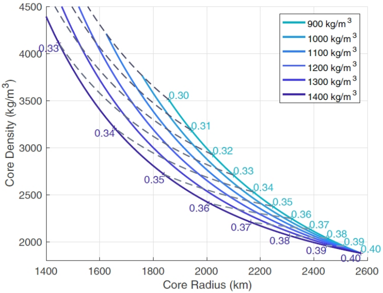

Interior models based on mass

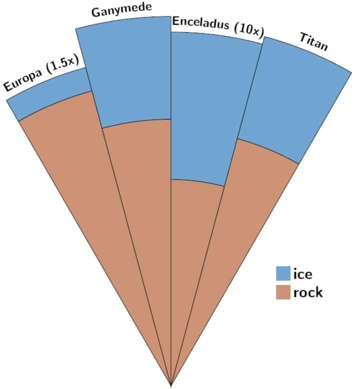

Interior models based on mass and MoI

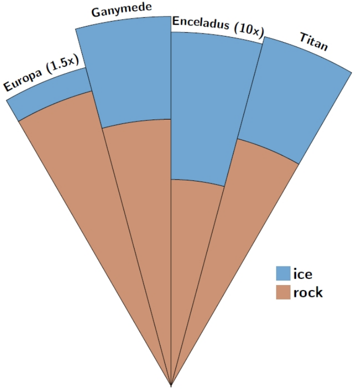

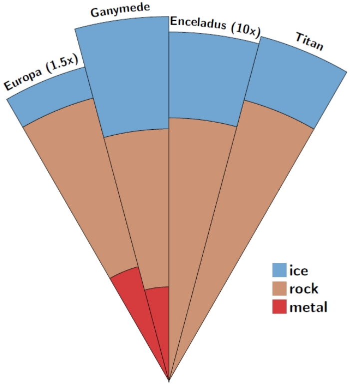

Interior models based on mass and MoI

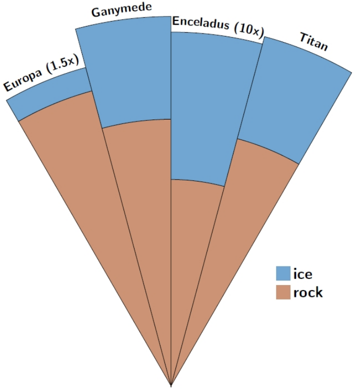

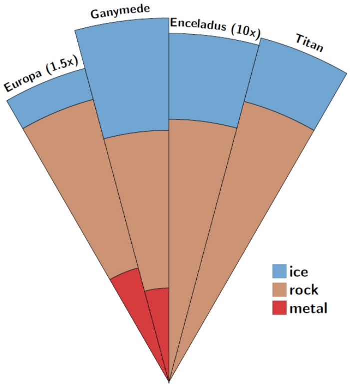

models taking into account the gravity field:

- Europa and Ganymede: iron cores, slightly thicker hydrospheres
- Enceladus and Titan: thinner hydrospheres → low core densities
- hydrated silicates
- porous material: Enceladus (*Choblet* +, 2017)
- organic material: Titan (*Néri* +, in rev.)

Course overview

1. Motivation - why do we study icy moons.
   History of exploration - telescope observations, spacecraft missions.
   Surface characteristics - composition, age, and morphology.

2. Interior structure - layered models: from gravity, shape, composition.
   Hydrosphere structure - H_2O phase diagram, presence of oceans.
   Preferred models for selected satellites.

3. Dynamics of the different planetary layers.
   Thermal evolution - heat sources, heat transfer.
   Melting/crystallization, anti-freezers.
   Implications for the long-term stability of subsurface oceans.

4. Selected applications.
   Overview of future missions.

Presence of deep ocean

- due to small density difference between ice and liquid water, presence of the ocean cannot be inferred from the mass and gravity data
- other evidence for liquid water ocean:

- induced magnetic field
- auroral ovals oscillation
- Schumann resonance
- libration & obliquity
- tidal deformation
- heat flux
- surface activity
- ...

Induced magnetic field

(*Khurana* +, 2009)

- Faraday: time-varying mg. field accompanied by (time-var) el. field
- conductor in time-varying mg field: surface eddy currents induce secondary field that reduces primary field in the conductor

Induced magnetic field

(*Khurana* +, 2009)

- Faraday: time-varying mg. field accompanied by (time-var) el. field
- conductor in time-varying mg field: surface eddy currents induce secondary field that reduces primary field in the conductor
- uniform primary field, dipolar induced field (same frequency)
- primary + induced field avoids the moon

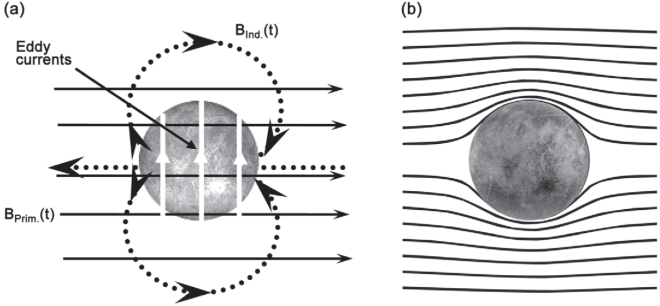

Induced magnetic field

(*Khurana* +, 2009)

- Faraday: time-varying mg. field accompanied by (time-var) el. field
- conductor in time-varying mg field: surface eddy currents induce secondary field that reduces primary field in the conductor
- uniform primary field, dipolar induced field (same frequency)
- primary + induced field avoids the moon
- elmg induction: detection & characterisation of secondary field

→ information on location, size, shape, and conductivity

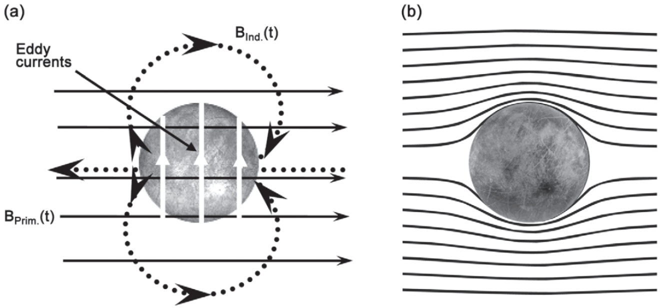

Induced magnetic field

(*Khurana* +, 2009)

- Jupiter's mg field: dipole tilted by ~9.6° → primary oscillating field
- additionally: day/night asymmetry in Jupiter's magnetospheric field
- Saturn's mg field: not inclined wrt rotation axis → moons do not sense a systematic time-periodic field in their rest frame

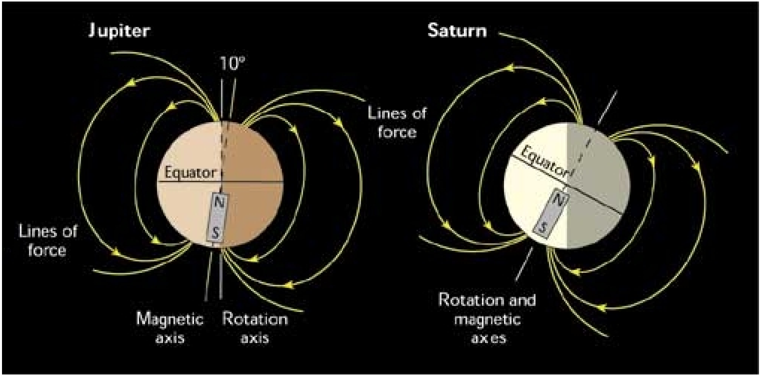

Induced magnetic field

(*Khurana* +, 2009)

- skin depth: distance over which the primary signal decays to 1/e

$$S = (\omega \mu_0 \sigma / 2)^{-1/2}$$

- small: large material conductivity and/or high sounding frequency
- obstacle thickness $> S$: primary wave reflection $\rightarrow$ induced field

Induced magnetic field

(*Khurana* +, 2009)

- skin depth: distance over which the primary signal decays to 1/e

$$S = (\omega\mu_0\sigma/2)^{-1/2}$$

- small: large material conductivity and/or high sounding frequency
- obstacle thickness $>S$: primary wave reflection → induced field

- Jupiter spin period ~10 h:
  - pure ice/water skin depth: ~10^6 km $\gg R_E$ → no induction
  - ocean water skin depth: ~60 km → significant induction
- three-layered model can be used to model the moon's induction response

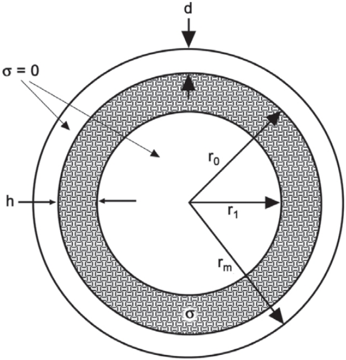

Induced magnetic field: Europa and Ganymede

(*Khurana* +, 1998; *Kivelson* +, 2000; *Kivelson* +, 2002; *Schilling* +, 2007)

Europa

- flybys with sufficiently low altitude required for an adequate signal-to-noise ratio to decipher the induced field
- strong evidence that Europa has a subsurface liquid water ocean
- best fit of Galileo data: ocean thickness < 100 km (cannot rule out thicker ocean)

Induced magnetic field: Europa and Ganymede

(*Khurana* +, 1998; *Kivelson* +, 2000; *Kivelson* +, 2002; *Schilling* +, 2007)

Europa

- flybys with sufficiently low altitude required for an adequate signal-to-noise ratio to decipher the induced field
- strong evidence that Europa has a subsurface liquid water ocean
- best fit of Galileo data: ocean thickness < 100 km (cannot rule out thicker ocean)

Ganymede

- discovery of intrinsic magnetic (*Kivelson*+, 1996)
- satisfactory fits of Galileo data:

(a) internal field with dipole and quadrupole terms

(b) internal permanent dipole

+ induced magnetic dipole from ocean ~150 km deep

- data did not allow to confirm the presence of an ocean

Ganymede: auroral ovals oscillation

(*Saur* +, 2015)

- auroral emission first observed by HST (*Hall* +, 1998)
- shape: two circumpolar auroral ovals in N & S polar regions
- location: open-closed field line boundary - separates mg field lines starting & ending on Ganymede from field lines connecting to Jupiter
- locations controlled by time-variable mg environment → oscillations
- ocean: primary field reduced by induced field → oscillation reduction

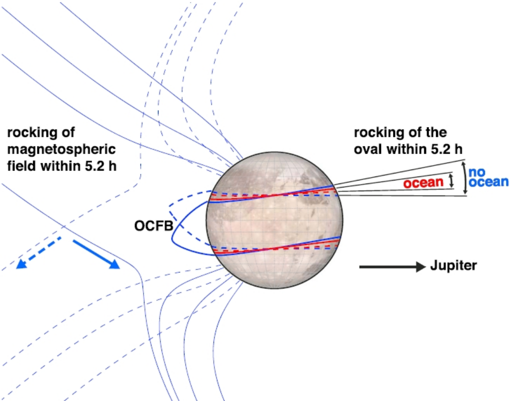

Ganymede: auroral ovals oscillation

(*Saur* +, 2015)

- auroral emission first observed by HST (*Hall* +, 1998)
- shape: two circumpolar auroral ovals in N & S polar regions
- location: open-closed field line boundary - separates mg field lines starting & ending on Ganymede from field lines connecting to Jupiter
- locations controlled by time-variable mg environment → oscillations
- ocean: primary field reduced by induced field → oscillation reduction

- HST observations: average oscillation of $2.0° \pm 1.3°$
- model:
- withouth ocean $5.8° \pm 1.3°$
- with ocean $2.2° \pm 1.3°$
- ocean depth ~150–250 km

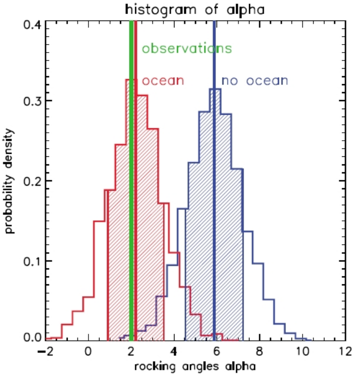

Evidence for ocean: Enceladus

1. geysers emanating from Enceladus' south pole → existence of water reservoir beneath the surface - regional sea/global ocean?

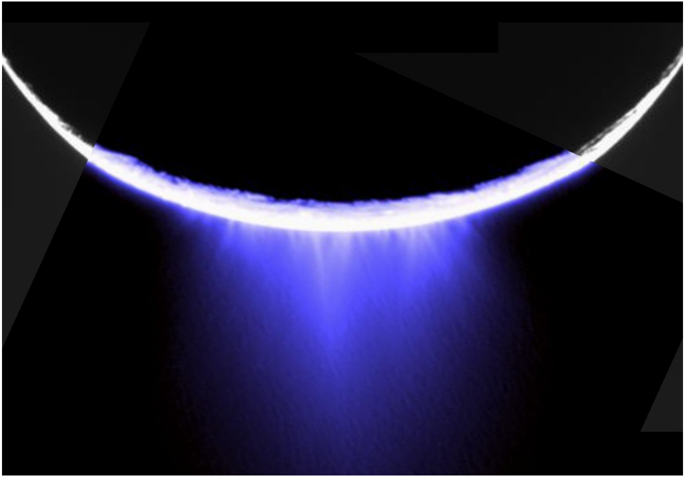

Evidence for ocean: Enceladus

1 geysers emanating from Enceladus' south pole → existence of water reservoir beneath the surface - regional sea/global ocean?

- ▸ synchronously rotating satellite on eccentric orbit:
- \- long axis points into empty focus: optical libration (Ψ)
- → periodic misalignement (long axis vs satellite-planet line)
- → gravitational torque → oscillations: physical longitudinal libration (γ)
- ▸ amplitude of γ depends on satellite's interior structure

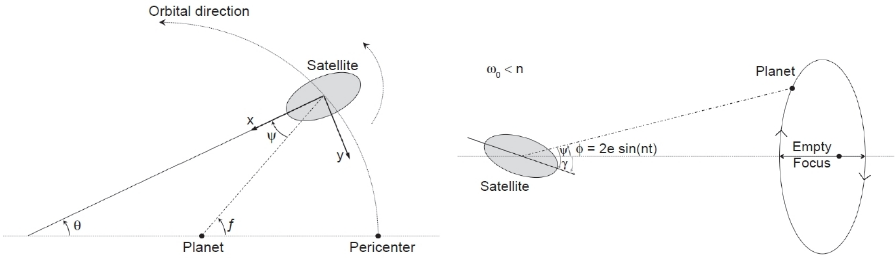

(credits: *Hemingway* +, 2018)

Evidence for ocean: Enceladus

1 geysers emanating from Enceladus' south pole → existence of water reservoir beneath the surface - regional sea/global ocean?

- *Thomas* + (2016):

- 488 points tracked through 340 images → $\gamma = 0.120° \pm 0.014°$

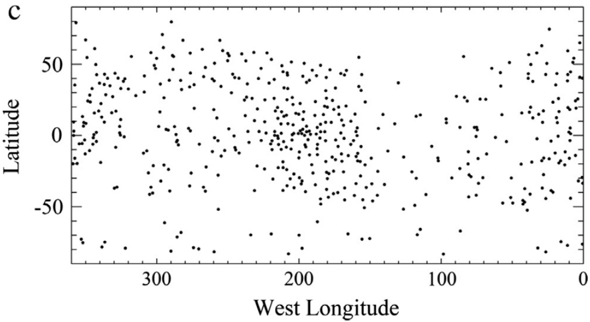

Evidence for ocean: Enceladus

1 geysers emanating from Enceladus' south pole → existence of water reservoir beneath the surface - regional sea/global ocean?

- *Thomas* + (2016):
- 488 points tracked through 340 images → $\gamma = 0.120° \pm 0.014°$
- too large for Enceladus' core being rigidly connected to its surface

Interior model	Amplitude of forced libration
Homogeneous ellipsoid	0.032°
2-layer hydrostatic	$0.032^\circ - 0.034^\circ$
2-layer hydrostatic, including "polar sea" and depression	$0.032^\circ - 0.034^\circ$
Ellipsoidal core, global ocean, ellipsoidal shell (23 km) (2300, 1000, 850 kg/m^3)	0.120°
Measured value	$0.120^\circ \pm 0.014^\circ$

Evidence for ocean: Enceladus

1. geysers emanating from Enceladus' south pole → existence of water reservoir beneath the surface - regional sea/global ocean?

- *Thomas* + (2016):
- 488 points tracked through 340 images → $\gamma = 0.120° \pm 0.014°$
- too large for Enceladus' core being rigidly connected to its surface

2. presence of a global ocean rather than a localized polar sea

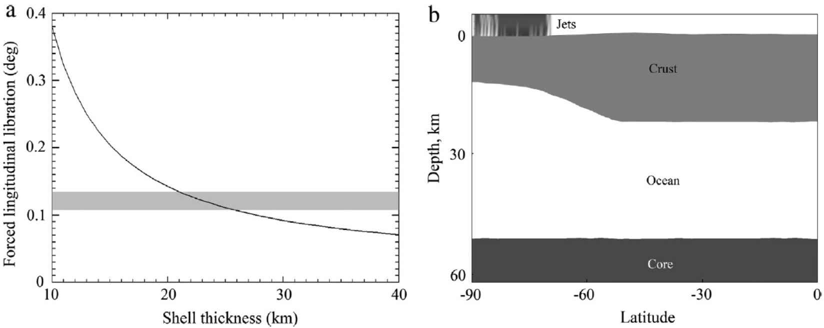

Evidence for ocean: Titan

(*Béghin* +, 2012)

1 Schumann resonance

- Earth:
  - global elmg resonance with extremely low frequency (ELF, 3–60 Hz)
  - in the cavity formed between the Earth's surface and the ionosphere
  - excited by lightning discharges
  - modes: 7.83 Hz (fundamental), 14.3, 20.8, 27.3 and 33.8 Hz

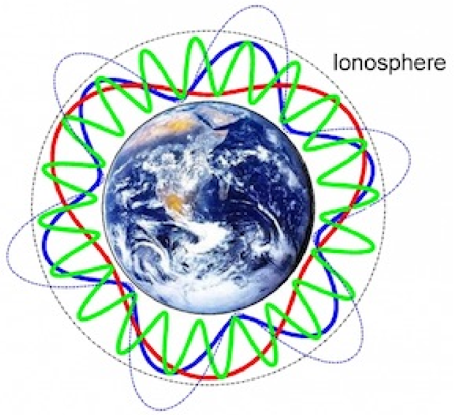

Evidence for ocean: Titan

(*Béghin* +, 2012)

1. Schumann resonance

- Titan - descent of Huygens probe:
- observed ELF (36 Hz) wave: 2nd harmonic of Schumann resonance
- resonating cavity: between layered ionosphere (up to 150 km height) and lower conductive surface beneath non-conductive ground
- excitation: ionospheric current sources
- lower reflector: water-ammonia ocean ~55–80 km below icy crust

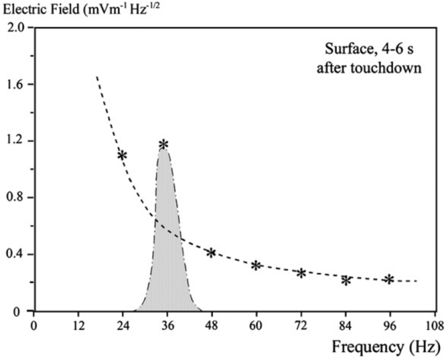

Evidence for ocean: Titan

(*Iess* +, 2012)

1 Schumann resonance (*Béghin* +, 2012)

2 tides

- eccentricity of Titan's orbit (~2.9%)

→ short-term time variation of quadrupole tidal forcing

→ change in Titan's shape and gravity

Evidence for ocean: Titan

(*Iess* +, 2012)

1 Schumann resonance (*Béghin* +, 2012)

2 tides

- eccentricity of Titan's orbit (~2.9%)

→ short-term time variation of quadrupole tidal forcing

→ change in Titan's shape and gravity

- k_2 (tidal) Love number: ratio of perturbed and perturbing potential

~ mass redistribution inside the body in response to forcing potential

- incompressible body: $k_2 = 3/2$, perfectly rigid body: $k_2 = 0$

Evidence for ocean: Titan

(*Iess* +, 2012)

1 Schumann resonance (*Béghin* +, 2012)

2 tides

- eccentricity of Titan's orbit (~2.9%)

→ short-term time variation of quadrupole tidal forcing

→ change in Titan's shape and gravity

- k_2 (tidal) Love number: ratio of perturbed and perturbing potential

~ mass redistribution inside the body in response to forcing potential

- incompressible body: $k_2 = 3/2$, perfectly rigid body: $k_2 = 0$

- 2 independent determinations from Cassini gravity data: $k_2 = 0.589 \pm 0.150$, $k_2 = 0.637 \pm 0.224$

→ some global layer within Titan behaves like a fluid on orbital time scales

(i) very low viscosity layer (an ocean) beneath an outer ice shell

(ii) low viscosity deep interior

Evidence for ocean: Titan

(*Baland* +, 2011)

1 Schumann resonance (*Béghin* +, 2012)

2 tides (*Iess* +, 2012)

3 obliquity (axial tilt)

- angle between satellite's rotational and orbital axis (~ angle between its equatorial and orbital plane)

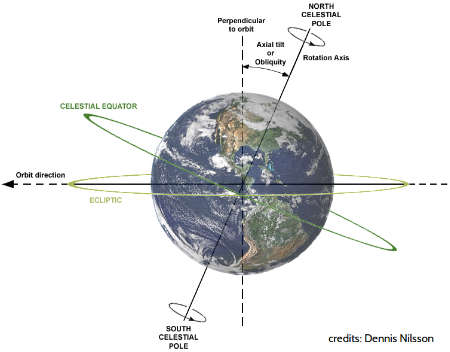

credits: Dennis Nilsson

Evidence for ocean: Titan

(*Baland* +, 2011)

1. Schumann resonance (*Béghin* +, 2012)
2. tides (*Iess* +, 2012)
3. obliquity (axial tilt)

- angle between satellite's rotational and orbital axis (~ angle between its equatorial and orbital plane)

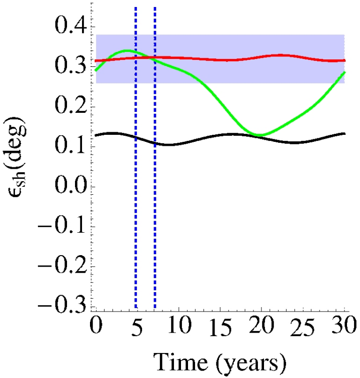

- Titan's obliquity: ε~0.3° (*Seidelmann* +, 2007)
- models: (*Baland* +, 2011)
- completely solid Titan: $\varepsilon = 0.12° \pm 0.02°$
- Titan with a liquid ocean: $\varepsilon = 0.32° \pm 0.02°$

→ another indirect evidence for Titan's subsurface ocean

Structure of the hydrosphere - H_2O phase diagram

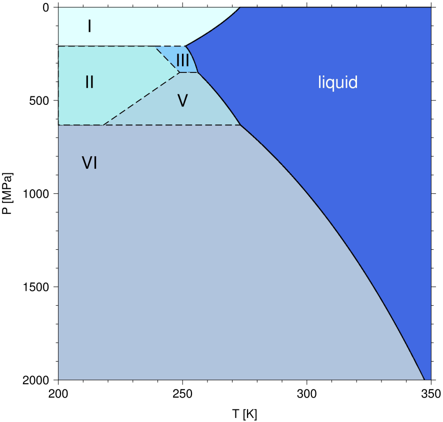

Structure of the hydrosphere - H_2O phase diagram

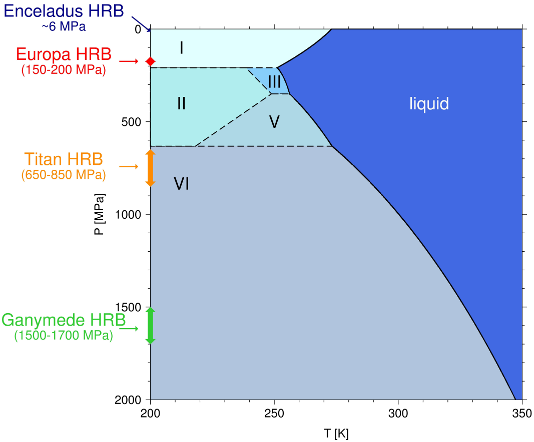

- hydrosphere-rock boundary (HRB):
- Europa, Enceladus: ice I
- Ganymede, Titan: high-pressure (HP) ices

Structure of the hydrosphere - H_2O phase diagram

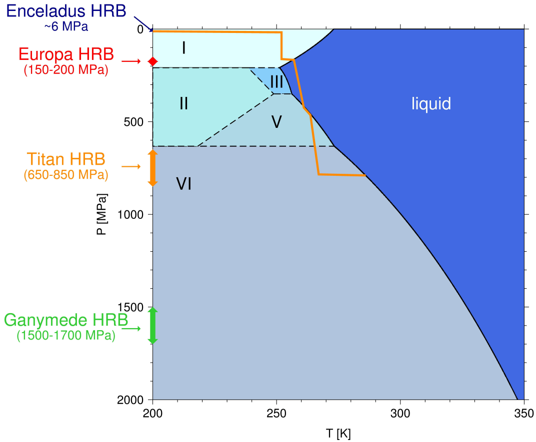

- hydrosphere-rock boundary (HRB):
- Europa, Enceladus: ice I
- Ganymede, Titan: high-pressure (HP) ices

→ liquid water ocean sandwiched between two ice layers

Updated interior structures

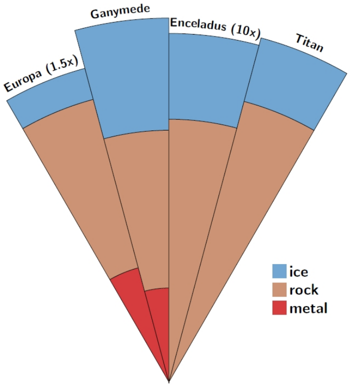

Updated interior structures

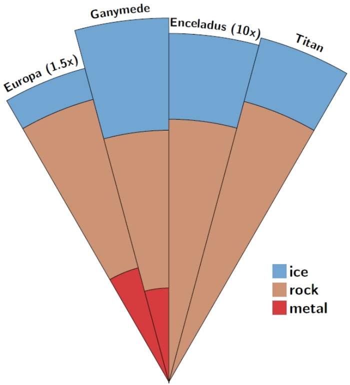

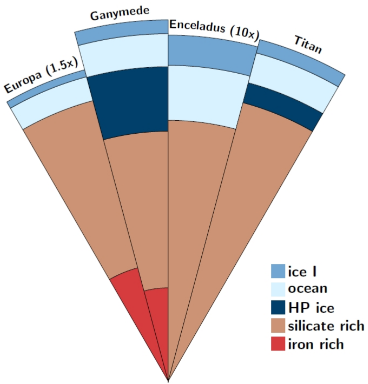

Updated interior structures

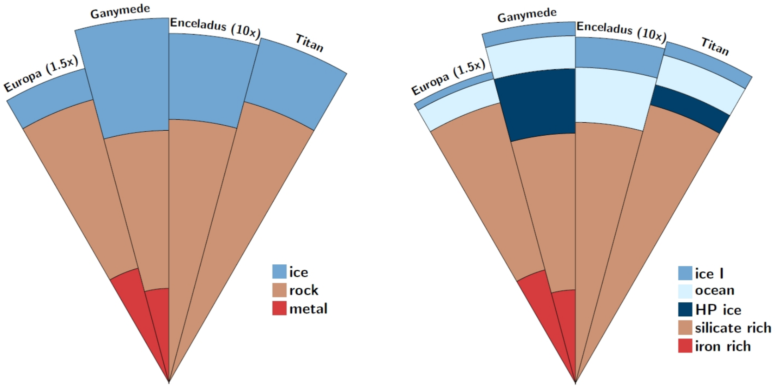

- Europa, Enceladus: ocean in direct contact with rock
- Ganymede, Titan: high-pressure ice decouples ocean from the rock

Updated interior structures

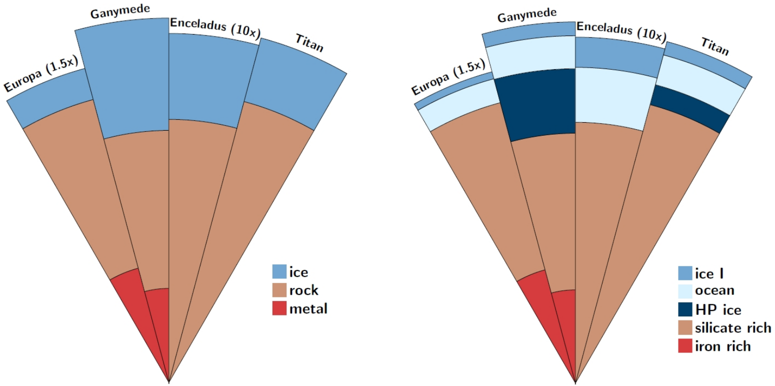

- Europa, Enceladus: ocean in direct contact with rock

→ great for origin of life ☺

- Ganymede, Titan: high-pressure ice decouples ocean from the rock

→ not so great for origin of life ☹

Adding more complexity

So far, we have assumed that:

- densities in particular layers are constant
- pure water/ice

Adding more complexity

So far, we have assumed that:

- densities in particular layers are constant
- pure water/ice

In reality:

- density changes with mineralogy that depends on (P,T)

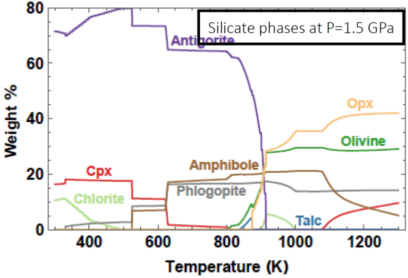

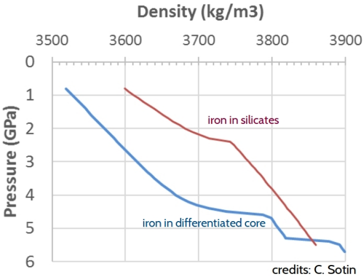

Adding more complexity

So far, we have assumed that:

- densities in particular layers are constant
- pure water/ice

In reality:

- density changes with mineralogy that depends on (P,T)
- salts (NaCl, $MgSO_4$, ...) and/or ammonia in the subsurface oceans

→ reduction of melting temperature

→ change of liquid water buoyancy

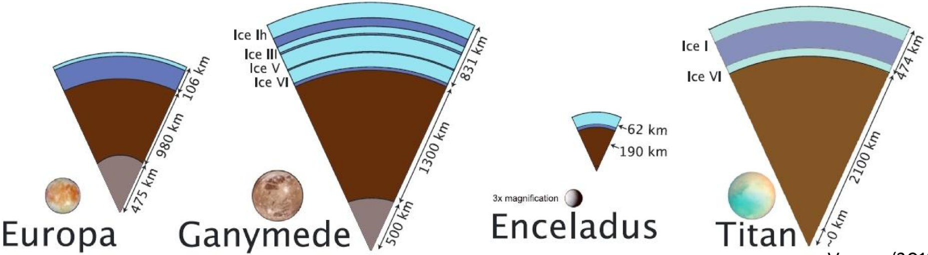

Vance + (2018)

Course overview

1. Motivation - why do we study icy moons.
   History of exploration - telescope observations, spacecraft missions.
   Surface characteristics - composition, age, and morphology.

2. Interior structure - layered models: from gravity, shape, composition.
   Hydrosphere structure - H_2O phase diagram, presence of oceans.
   Preferred models for selected satellites.

3. Dynamics of the different planetary layers.
   Thermal evolution - heat sources, heat transfer.
   Melting/crystallization, anti-freezers.
   Implications for the long-term stability of subsurface oceans.

4. Selected applications.
   Overview of future missions.

Preferred interior models for selected satellites

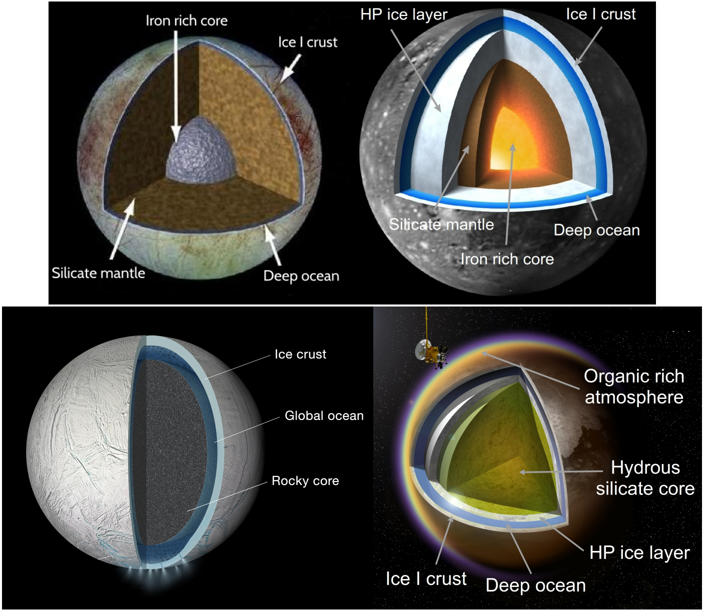

References

books:

Europa, eds. Pappalardo, McKinnon, Khurana, U. Arizona Press, 2009.

- Khurana et al., Electromagnetic induction from Europa's ocean and the deep interior, 571–588.
- Schubert et al., Interior of Europa, 353–367.

Enceladus and the Icy Moons of Saturn, eds. Schenk, Clark, Howett, Verbiscer, Waite, U. Arizona Press, 2018.

- Hemingway et al., The interior of Enceladus, 57–78.

papers:

- Anderson et al. (1996), *Nature*, **384**, 541–543.
- Anderson et al. (1998), *Science*, **281**, 2019–2022.
- Baland et al. (2011), *Astron. Astrophys.*, **530**, 6.
- Béghin et al. (2012), *Icarus*, **218**, 1028–1042.
- Choblet et al. (2017), *Nature Astron*, **1**, 841–847.
- Durante et al. (2019), *Icarus*, **326**, 123–132.

References

- Dziewonski & Anderson (1981), *Phys. Earth Planet. Int.*, **25**, 297–356.
- Hall et al. (1998), *Astrophys. J.*, **499**, 475–481.
- Hubbard & Anderson (1978), *Icarus*, **33**, 336–341.
- Hussmann et al. (2015), in: Treatise on Geophysics, Elsevier, 605–635.
- Iess et al. (2012), *Science*, **337**, 457–459.
- Iess et al. (2014), *Science*, **344**, 78–80.
- Khurana et al. (1998), *Nature*, **395**, 777–780.
- Kivelson et al. (1996), *Nature*, **384**, 537–541.
- Kivelson et al. (2000), *Science*, **289**, 1340–1343.
- Kivelson et al. (2002), *Icarus*, **157**, 507–522.
- Néri et al., *Earth Planet. Sci. Lett.*, under review.
- Saur et al. (2015), *J. Geophys. Res.*, **120**(3), 1715–1737.
- Schilling et al. (2007), *Icarus*, **192**, 41–55.
- Seidelmann et al. (2007), *Transactions of the IAU, Series A*, **26**, 181.
- Stein & Wysession (2003), Oxford: Blackwell (isbn 0865420785).
- Thomas et al. (2016), *Icarus*, **264**, 37–47.
- Vance et al. (2018), *J. Geophys. Res.*, **123**, 180–205.